

Photophysical properties of new *p*-phenylene- and benzodithiophene-based fluorophores for luminescent solar concentrators (LSCs)

Gianluigi Albano^{a,1}, Tony Colli^a, Tarita Biver^{a,b}, Laura Antonella Aronica^a, Andrea Pucci^{a,c,*}

^a Dipartimento di Chimica e Chimica Industriale, Università di Pisa, Via Giuseppe Moruzzi 13, 56124, Pisa, Italy

^b Dipartimento di Farmacia, Università di Pisa, Via Bonanno 6, 56126, Pisa, Italy

^c INSTM, UdR Pisa, Via Giuseppe Moruzzi 13, 56124, Pisa, Italy

ARTICLE INFO

Keywords:

Luminescent solar concentrator
Organic dye
Optical efficiency
Solvatochromism
Benzodithiophene
Sonogashira reaction

ABSTRACT

In this study, we report on the synthesis of new organic fluorophores containing either the *p*-phenylene or the benzodithiophene cyclic nucleus connected to thiophene units via triple bonds and carbonyl group, and on their application for the fabrication of luminescent solar concentrators (LSCs). Their optical properties were evaluated. Independent of the core, dyes containing the CO-thiophene residues seem to be the most promising for LSCs applications. In fact, carbonyl groups slightly enhance the quantum yield but significantly increase the red-shift of the emission so that the superimposition between the absorbance spectrum and the emission one is diminished. In the case of the benzodithiophene centre, light emission in the yellow-red portion of the spectrum is achieved. The latter dye is then selected for tests in a poly(methyl methacrylate) (PMMA) matrix. It showed good compatibility and homogenous distribution, no auto-absorption phenomena, and optical efficiencies of about 8% at 1 wt. %, i.e. comparable with those PMMA/Lumogen Red films in the same range of concentration.

1. Introduction

Recently, high attention has been paid to climate changes due to CO₂ emissions generated from carbon-based fuels. As a consequence, renewable energy sources have become a hot topic in the research community. One of the most widespread technologies of renewable energy generation is the use of photovoltaic (PV) systems which convert sunlight into useable electrical energy [1]. PV technology is unique in its extreme scalability, ranging from watt-scale individual systems to kilowatt- and megawatt-scale distributed domestic and industrial power systems and to power plants of hundreds of megawatts.

Solar cells produce a quantity of electrical energy directly proportional to the total power of the absorbed light. Hence, if the intensity of the incident light is increased a linear response in energy production will be observed: this is the principle on which geometric solar concentrators are based [2–4]. These devices can concentrate the light on small and highly efficient photovoltaic solar cells, thus lowering the cost of energy by reducing cell surfaces. Nevertheless, optical concentrators have some disadvantages such as the need of rotation mechanisms that allow the concentrator to follow the Sun's apparent motion, and a cooling system to disperse the excess heat due to unconverted energy [5,6]. To

compensate for these defects luminescent solar concentrators (LSCs) were developed [7–13].

LSCs generally consist of an inert material (often a polymer [14]) containing a suitable dye which, once exposed to sunlight, converts part of the absorbed radiation into a longer emitting wavelength by fluorescence. The reemitted light can be concentrated via total internal reflection in the optical waveguide construction. Therefore, solar cells attached to LSC can generate more electric power than conventionally used ones. The emitting dyes are the driving force for light concentration in LSCs cells. There are three main kinds of fluorophores: quantum dots [15–18], lanthanide-based materials [19,20] and organic dyes. Respect to the two first classes of compounds, organic dyes are usually less toxic and their optical properties (Stokes shift, quantum yield, thermal- and photo-stability) can be optimized by modifying the structure of organic molecules. Many of them possess one or more heterocyclic nuclei such as thiazoles, imidazoles, benzothiazoles, benzodithiophenes, oxazines, lactones, pyrans, pyrroles, thiophenes, pyridines, pyrimidines, and dithienosiloles [21–34].

Recently we have reported [35] that dimethoxy-1,4-phenylene unit linked to two (thiophen-2-yl)prop-2-yn-1-one moieties connected to a PV cell showed optical efficiency of 6.2%, thus supporting the use of this

* Corresponding author. Dipartimento di Chimica e Chimica Industriale, Università di Pisa, Via Giuseppe Moruzzi 13, 56124, Pisa, Italy.

E-mail address: andrea.pucci@unipi.it (A. Pucci).

¹ Present address: Dipartimento di Chimica, Università degli Studi di Bari "Aldo Moro", Via Edoardo Orabona 4, 70,126 Bari, Italy.

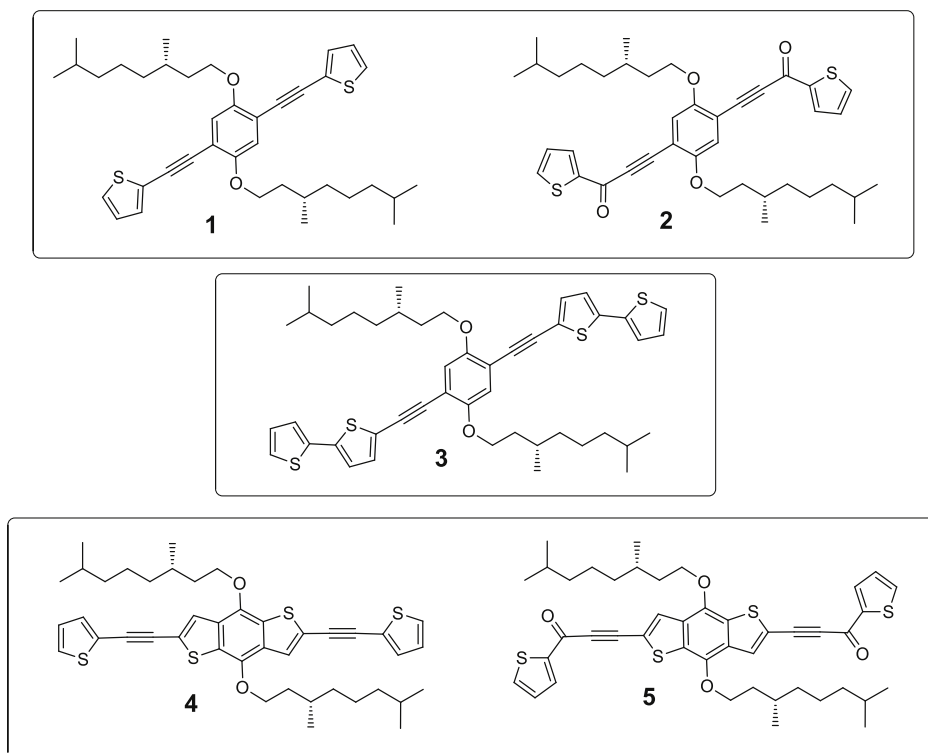


Fig. 1. Chemical structure of the five new fluorophores studied in this work.

compound as a fluorophore for colourless LSC devices.

Prompted by these promising results, here we describe the synthesis of five new fluorophores containing an electron-rich nucleus linked to thiophene rings via $\text{C}\equiv\text{C}$ or $\text{C}\equiv\text{C}-\text{C}=\text{O}$ bridges (Fig. 1) and the study of their optical properties both in solution and in polymer films.

2. Experimental section

2.1. Materials and apparatus

Solvents were purified by conventional methods, distilled and stored over activated molecular sieves under argon. Poly(methyl methacrylate) (PMMA, Aldrich, MW = 350,000 g/mol, acid number < 1 mg KOH/g) was used as received. All the other chemicals were purchased from commercial sources and used as received without purification. All the operations under inert atmosphere were carried out using standard Schlenk techniques and employing dried nitrogen. For all reactions, conversion was monitored by thin-layer chromatography (TLC) analysis on pre-coated silica gel plates ALUGRAM® Xtra SIL G/UV₂₅₄ (0.2 mm) purchased from VWR Macherey-Nagel. Column chromatographies were performed with Fluka silica gel, pore size 60 Å, 70–230 mesh, 63–200 µm. ¹H NMR and ¹³C NMR spectra were recorded at room temperature in CDCl₃ or DMSO-*d*₆ solution with a Bruker Avance DRX 400 spectrometer, operating at a frequency of 400 MHz for ¹H and 100 MHz for ¹³C, using the residual solvent peak as internal reference; chemical shifts (δ) values are given in parts per million (ppm) and coupling constants (*J*) in Hertz. Mass spectra were obtained with an Applied Biosystems-MDS Sciex API 4000 triple quadrupole mass spectrometer (Concord, Ont., Canada), equipped with a Turbo-V ion-spray (TIS) source. Elemental analyses were performed on a Elementar Vario Micro Cube CHN-analyzer.

2.2. Synthesis of *p*-phenylene-based fluorophores

2.2.1. Synthesis of 1,4-bis((*S*)-3,7-dimethyloctyloxy)-2,5-bis(trimethylsilyl)ethynylbenzene (9)

1,4-Bis((*S*)-3,7-dimethyloctyloxy)-2,5-diiodobenzene (6) (1.00 g, 1.56 mmol), Pd(PPh₃)₄ (90 mg, 0.078 mmol), CuI (30 mg, 0.157 mmol) and Et₃N (15 mL) were mixed together, then trimethylsilylacetylene (8) (766 mg, 7.8 mmol) was added dropwise. The resulting mixture was refluxed under stirring for 7 h, then it was cooled to room temperature, hydrolyzed with saturated ammonium chloride solution (20 mL) and extracted with CH₂Cl₂ (3 × 30 mL). The combined organic phases were washed with brine (50 mL), dried over anhydrous Na₂SO₄ and the solvent was removed under vacuum. The crude product was purified by column chromatography (SiO₂, *n*-pentane) to give 1,4-bis((*S*)-3,7-dimethyloctyloxy)-2,5-bis(trimethylsilyl)ethynylbenzene (9) (900 mg, yield 99%) as an orangish oil. ¹H NMR (400 MHz, CDCl₃), δ (ppm): 0.25 (18H, s), 0.87 (12H, d, *J* = 6.7 Hz), 0.95 (6H, d, *J* = 6.6 Hz), 1.11–1.20 (6H, m), 1.26–1.37 (6H, m), 1.48–1.62 (4H, m), 1.71–1.79 (2H, m), 1.80–1.88 (2H, m), 3.94–4.02 (4H, m), 6.90 (2H, s). ¹³C NMR (100 MHz, CDCl₃), δ (ppm): −0.06 (3C), 19.65, 22.56, 22.68, 24.72, 27.95, 29.76, 36.26, 37.34, 39.29, 67.72, 99.98, 101.08, 113.92, 117.16, 153.99. LC-MS (APCI⁺), *m/z*: 583.61 [M+H]⁺. Anal. calcd for C₃₆H₆₂O₂Si₂: C, 74.16; H, 10.72; found: C, 74.29; H, 10.59.

2.2.2. Synthesis of 1,4-bis((*S*)-3,7-dimethyloctyloxy)-2,5-diethynylbenzene (10)

1,4-Bis((*S*)-3,7-dimethyloctyloxy)-2,5-bis(trimethylsilyl)ethynylbenzene (9) (900 mg, 1.54 mmol), 3 M KOH aqueous solution (1.2 mL, 3.6 mmol), THF (68 mL) and methanol (22 mL) were mixed together. The resulting mixture was left under stirring for 7 h at room temperature, then it was hydrolyzed with H₂O (60 mL) and extracted with CH₂Cl₂ (3 × 60 mL). The combined organic phases were washed with brine (100 mL), dried over anhydrous Na₂SO₄ and the solvent was removed under vacuum. The crude product was purified by column chromatography (SiO₂, petroleum ether/CH₂Cl₂ 4:1) to give 1,4-bis((*S*)-

3,7-dimethyloctyloxy)-2,5-diethynylbenzene (**10**) (507 mg, yield 75%) as a orangish oil. ^1H NMR (400 MHz, CDCl_3), δ (ppm): 0.86 (12H, d, $J = 6.7$ Hz), 0.94 (6H, d, $J = 6.7$ Hz), 1.11–1.24 (6H, m), 1.25–1.37 (6H, m), 1.48–1.64 (4H, m), 1.64–1.76 (2H, m), 1.81–1.89 (2H, m), 3.32 (2H, s), 3.96–4.05 (4H, m), 6.96 (2H, s). ^{13}C NMR (100 MHz, CDCl_3), δ (ppm): 19.70, 22.59, 22.68, 24.65, 27.95, 29.80, 36.02, 37.23, 39.18, 67.97, 79.79, 82.40, 113.20, 117.60, 153.97. LC-MS (APCI $^+$), m/z : 439.57 $[\text{M}+\text{H}]^+$. Anal. calcd for $\text{C}_{30}\text{H}_{46}\text{O}_2$: C, 82.14; H, 10.57; found: C, 82.19; H, 10.63.

2.2.3. Synthesis of 1,4-bis((S)-3,7-dimethyloctyloxy)-2,5-bis(thiophen-2-ylethynyl)benzene (**1**)

1,4-Bis((S)-3,7-dimethyloctyloxy)-2,5-diethynylbenzene (**10**) (150 mg, 0.34 mmol), 2-iodothiophene (164 mg, 0.78 mmol), $\text{Pd}(\text{PPh}_3)_4$ (20 mg, 0.017 mmol), CuI (7 mg, 0.037 mmol) and Et_3N (15 mL) were mixed together. The resulting mixture was refluxed under stirring for 24 h, then it was cooled to room temperature, hydrolyzed with saturated ammonium chloride solution (20 mL) and extracted with CH_2Cl_2 (3 \times 30 mL). The combined organic phases were washed with brine (50 mL), dried over anhydrous Na_2SO_4 and the solvent was removed under vacuum. The crude product was purified by column chromatography (SiO_2 , petroleum ether/ CH_2Cl_2 4:1) to give 1,4-bis((S)-3,7-dimethyloctyloxy)-2,5-bis(thiophen-2-ylethynyl)benzene (**1**) (189 mg, yield 92%) as a yellowish oil. ^1H NMR (400 MHz, CDCl_3), δ (ppm): 0.88 (12H, d, $J = 6.6$ Hz), 1.01 (6H, d, $J = 6.6$ Hz), 1.15–1.23 (6H, m), 1.31–1.41 (6H, m), 1.50–1.59 (2H, m), 1.62–1.70 (2H, m), 1.76–1.84 (2H, m), 1.88–1.96 (2H, m), 4.03–4.12 (4H, m), 7.02–7.04 (4H, m), 7.30–7.32 (4H, m). ^{13}C NMR (100 MHz, CDCl_3), δ (ppm): 19.70, 22.57, 22.68, 24.74, 27.94, 29.88, 36.23, 37.34, 39.22, 67.90, 88.06, 89.77, 113.71, 116.40, 123.48, 127.06, 127.33, 131.77, 153.46. LC-MS (APCI $^+$), m/z : 603.45 $[\text{M}+\text{H}]^+$. Anal. calcd for $\text{C}_{38}\text{H}_{50}\text{O}_2\text{S}_2$: C, 75.70; H, 8.36; S, 10.64; found: C, 75.86; H, 8.31; S, 10.63.

2.2.4. Synthesis of 3,3'-(2,5-bis((S)-3,7-dimethyloctyloxy)-1,4-phenylene)bis(1-(thiophen-2-yl)prop-2-yn-1-one) (**2**)

1,4-Bis((S)-3,7-dimethyloctyloxy)-2,5-diethynylbenzene (**10**) (150 mg, 0.34 mmol), thiophene-2-carbonyl chloride (145 mg, 0.99 mmol), $\text{Pd}(\text{PPh}_3)_4$ (20 mg, 0.017 mmol) and Et_3N (15 mL) were mixed together. The resulting mixture was left under stirring for 24 h at 50 $^\circ\text{C}$, then it was cooled to room temperature, hydrolyzed with saturated ammonium chloride solution (20 mL) and extracted with CH_2Cl_2 (3 \times 30 mL). The combined organic phases were washed with brine (50 mL), dried over anhydrous Na_2SO_4 and the solvent was removed under vacuum. The crude product was purified by column chromatography (SiO_2 , *n*-hexane/ CH_2Cl_2 1:1) to give 3,3'-(2,5-bis((S)-3,7-dimethyloctyloxy)-1,4-phenylene)bis(1-(thiophen-2-yl)prop-2-yn-1-one) (**2**) (157 mg, yield 70%) as a yellow solid. ^1H NMR (400 MHz, CDCl_3), δ (ppm): 0.84 (12H, d, $J = 6.6$ Hz), 0.97 (6H, d, $J = 6.6$ Hz), 1.12–1.25 (6H, m), 1.28–1.38 (6H, m), 1.45–1.55 (2H, m), 1.68–1.78 (4H, m), 1.91–1.99 (2H, m), 4.04–4.13 (4H, m), 7.15–7.18 (4H, m), 7.74 (2H, dd, $J = 4.9, 1.3$ Hz), 8.15 (2H, dd, $J = 3.8, 1.3$ Hz). ^{13}C NMR (100 MHz, CDCl_3), δ (ppm): 19.51, 22.51, 22.63, 24.57, 27.88, 29.74, 36.22, 37.19, 39.15, 67.84, 87.71, 92.11, 112.93, 117.43, 128.11, 135.36, 136.12, 145.04, 154.91, 169.60. LC-MS (APCI $^+$), m/z : 659.31 $[\text{M}+\text{H}]^+$. Anal. calcd for $\text{C}_{40}\text{H}_{50}\text{O}_4\text{S}_2$: C, 72.91; H, 7.65; S, 9.73; found: C, 72.84; H, 7.69; S, 9.72.

2.2.5. Synthesis of 1,4-bis((S)-3,7-dimethyloctyloxy)-2,5-bis([2,2'-bithiophen]-5-ylethynyl)benzene (**3**)

1,4-Diiodo-2,5-bis((S)-3,7-dimethyloctyloxy)benzene (**6**) (470 mg, 0.73 mmol), 5-ethynyl-2,2'-bithiophene (**11**) (250 mg, 1.31 mmol), $\text{Pd}(\text{PPh}_3)_4$ (43 mg, 0.037 mmol), CuI (14 mg, 0.074 mmol) and Et_3N (60 mL) were mixed together. The resulting mixture was left under stirring at 35 $^\circ\text{C}$ for 24 h, then it was cooled to room temperature, hydrolyzed with a saturated ammonium chloride solution (50 mL) and extracted with CH_2Cl_2 (3 \times 70 mL). The combined organic phases were washed with brine (100 mL), dried over anhydrous Na_2SO_4 and the solvent was

removed under vacuum. The crude product was purified by column chromatography (SiO_2 , petroleum ether/ CH_2Cl_2 4:1) to give 1,4-bis((S)-3,7-dimethyloctyloxy)-2,5-bis([2,2'-bithiophen]-5-ylethynyl)benzene (**3**) (330 mg, yield 59%) as yellow solid. ^1H NMR (400 MHz, CDCl_3), δ (ppm): 0.88 (12H, d, $J = 6.6$ Hz), 1.02 (6H, d, $J = 6.6$ Hz), 1.15–1.47 (12H, m), 1.50–1.59 (2H, m), 1.61–1.73 (2H, m), 1.77–1.88 (2H, m), 1.89–2.00 (2H, m), 4.02–4.18 (4H, m), 7.02 (2H, s), 7.03–7.06 (2H, m), 7.10 (2H, d, $J = 4.0$ Hz), 7.20 (2H d, $J = 4.0$ Hz), 7.21–7.23 (2H, m), 7.26–7.28 (2H, m). ^{13}C NMR (100 MHz, CDCl_3), δ (ppm): 19.76, 22.61, 22.71, 24.82, 28.00, 29.96, 36.28, 37.41, 39.30, 67.99, 88.24, 90.96, 113.74, 116.34, 122.15, 123.61, 124.22, 125.00, 127.95, 132.72, 136.81, 139.08, 153.53. LC-MS (APCI $^+$), m/z : 767.30 $[\text{M}+\text{H}]^+$. Anal. calcd for $\text{C}_{46}\text{H}_{54}\text{O}_2\text{S}_4$: C, 72.02; H, 7.09; S, 16.72; found: C, 72.11; H, 7.03; S, 16.72.

2.3. Synthesis of benzo[1,2-b:4,5-b']dithiophene-based fluorophores

2.3.1. Synthesis of 2,6-bis(trimethylsilylethynyl)-4,8-bis((S)-3,7-dimethyloctyloxy)benzo[1,2-b:4,5-b']dithiophene (**12**)

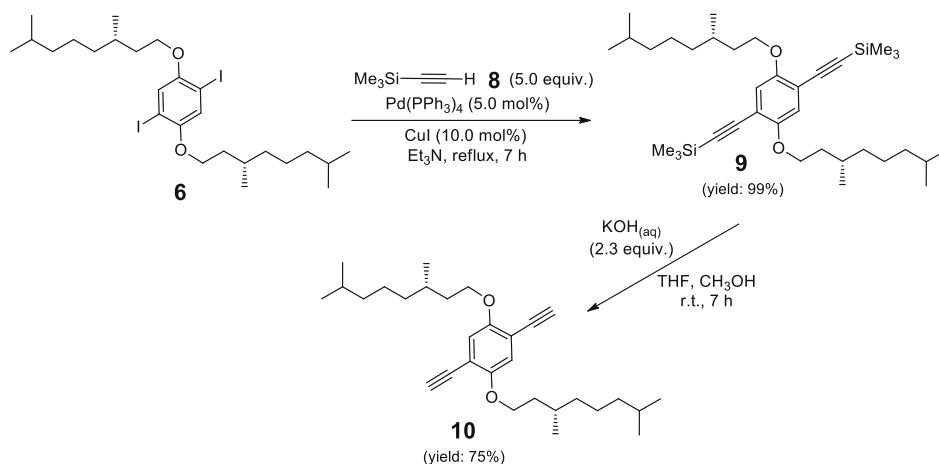
2,6-Dibromo-4,8-bis((S)-3,7-dimethyloctyloxy)benzo[1,2-b:4,5-b']dithiophene (**7**) (1.00 g, 1.51 mmol), $\text{Pd}(\text{PPh}_3)_4$ (88 mg, 0.076 mmol), CuI (29 mg, 0.152 mmol) and Et_3N (15 mL) were mixed together, then trimethylsilylacetylene (**8**) (445 mg, 4.53 mmol) was added dropwise. The resulting mixture was refluxed under stirring for 7 h, then it was cooled to room temperature, hydrolyzed with saturated ammonium chloride solution (20 mL) and extracted with CH_2Cl_2 (3 \times 30 mL). The combined organic phases were washed with brine (50 mL), dried over anhydrous Na_2SO_4 and the solvent was removed under vacuum. The crude product was purified by column chromatography (SiO_2 , *n*-hexane/ CH_2Cl_2 5:1) to give 2,6-bis(trimethylsilylethynyl)-4,8-bis((S)-3,7-dimethyloctyloxy)benzo[1,2-b:4,5-b']dithiophene (**12**) (976 mg, yield 93%) as a orangish oil. ^1H NMR (400 MHz, CDCl_3), δ (ppm): 0.27 (18H, s), 0.87 (12H, d, $J = 6.6$ Hz), 0.96 (6H, d, $J = 6.6$ Hz), 1.14–1.22 (6H, m), 1.29–1.41 (6H, m), 1.46–1.59 (2H, m), 1.60–1.69 (2H, m), 1.71–1.81 (2H, m), 1.82–1.92 (2H, m), 4.21–4.29 (4H, m), 7.57 (2H, s). ^{13}C NMR (100 MHz, CDCl_3), δ (ppm): -0.23 (3C), 19.75, 22.62, 22.73, 24.69, 27.96, 29.73, 37.25, 37.54, 39.23, 72.42, 97.77, 101.65, 122.91, 125.92, 130.09, 131.75, 143.88. LC-MS (APCI $^+$), m/z : 696.04 $[\text{M}+\text{H}]^+$. Anal. calcd for $\text{C}_{40}\text{H}_{62}\text{O}_2\text{S}_2\text{Si}_2$: C, 69.10; H, 8.99; S, 9.22; found: C, 68.97; H, 9.14; S, 9.23.

2.3.2. Synthesis of 2,6-diethynyl-4,8-bis((S)-3,7-dimethyloctyloxy)benzo[1,2-b:4,5-b']dithiophene (**13**)

2,6-Bis(trimethylsilylethynyl)-4,8-bis((S)-3,7-dimethyloctyloxy)benzo[1,2-b:4,5-b']dithiophene (**12**) (976 mg, 1.40 mmol), 3 M KOH aqueous solution (1.1 mL, 3.3 mmol), THF (68 mL) and methanol (22 mL) were mixed together. The resulting mixture was left under stirring for 7 h at room temperature, then it was hydrolyzed with H_2O (60 mL) and extracted with CH_2Cl_2 (3 \times 60 mL). The combined organic phases were washed with brine (100 mL), dried over anhydrous Na_2SO_4 and the solvent was removed under vacuum. The crude product was purified by column chromatography (SiO_2 , *n*-hexane/ CH_2Cl_2 5:2) to give 2,6-diethynyl-4,8-bis((S)-3,7-dimethyloctyloxy)benzo[1,2-b:4,5-b']dithiophene (**13**) (679 mg, yield 88%) as a brownish solid. ^1H NMR (400 MHz, CDCl_3), δ (ppm): 0.89 (12H, d, $J = 6.6$ Hz), 0.98 (6H, d, $J = 6.6$ Hz), 1.13–1.23 (6H, m), 1.24–1.44 (6H, m), 1.50–1.60 (2H, m), 1.62–1.72 (2H, m), 1.74–1.82 (2H, m), 1.87–1.95 (2H, m), 3.48 (2H, s), 4.23–4.32 (4H, m), 7.63 (2H, s). ^{13}C NMR (100 MHz, CDCl_3), δ (ppm): 19.71, 22.62, 22.72, 24.71, 27.97, 29.72, 37.27, 37.52, 39.24, 72.48, 77.26, 83.44, 121.93, 126.59, 130.13, 131.70, 144.00. LC-MS (APCI $^+$), m/z : 551.54 $[\text{M}+\text{H}]^+$. Anal. calcd for $\text{C}_{34}\text{H}_{46}\text{O}_2\text{S}_2$: C, 74.13; H, 8.42; S, 11.64; found: C, 74.26; H, 8.33; S, 11.64.

2.3.3. Synthesis of 4,8-bis((S)-3,7-dimethyloctyloxy)-2,6-bis(thiophen-2-ylethynyl)benzo[1,2-b:4,5-b']dithiophene (**4**)

2,6-Diethynyl-4,8-bis((S)-3,7-dimethyloctyloxy)benzo[1,2-b:4,5-b']



Scheme 1. Synthesis of 1,4-bis(((S)-3,7-dimethyloctyl)oxy)-2,5-diethynylbenzene (10).

dithiophene (13) (200 mg, 0.36 mmol), 2-iodothiophene (302 mg, 1.44 mmol), Pd(PPh₃)₂Cl₂ (13 mg, 0.019 mmol), CuI (7 mg, 0.037 mmol) and Et₃N (15 mL) were mixed together. The resulting mixture was left under stirring for 30 h at 50 °C, then it was cooled to room temperature, hydrolyzed with saturated ammonium chloride solution (20 mL) and extracted with CH₂Cl₂ (3 × 30 mL). The combined organic phases were washed with brine (50 mL), dried over anhydrous Na₂SO₄ and the solvent was removed under vacuum. The crude product was purified by column chromatography (SiO₂, petroleum ether/CH₂Cl₂ 9:1) to give 4,8-bis((S)-3,7-dimethyloctyloxy)-2,6-bis(thiophen-2-ylethynyl)benzo [1,2-*b*:4,5-*b'*]dithiophene (4) (193 mg, yield 75%) as a dark yellow solid. ¹H NMR (400 MHz, CDCl₃), δ (ppm): 0.88 (12H, d, *J* = 6.6 Hz), 0.99 (6H, d, *J* = 6.6 Hz), 1.14–1.27 (6H, m), 1.28–1.43 (6H, m), 1.51–1.60 (2H, m), 1.64–1.72 (2H, m), 1.75–1.83 (2H, m), 1.89–1.97 (2H, m), 4.26–4.35 (4H, m), 7.04–7.06 (2H, m), 7.34–7.37 (4H, m), 7.62 (2H, s). ¹³C NMR (100 MHz, CDCl₃), δ (ppm): 19.77, 22.64, 22.74, 24.73, 28.00, 29.78, 37.32, 37.58, 39.27, 72.50, 86.81, 88.68, 122.41, 122.71, 125.37, 127.31, 128.29, 130.34, 131.96, 132.74, 143.93. LC-MS (APCI⁺), *m/z*: 716.07 [M+H]⁺. Anal. calcd for C₄₂H₅₀O₂S₄: C, 70.54; H, 7.05; S, 17.94; found: C, 70.61; H, 7.01; S, 17.93.

2.3.4. Synthesis of 3,3'-(4,8-bis((S)-3,7-dimethyloctyloxy)benzo[1,2-*b*:4,5-*b'*]dithiophene-2,6-diyl)bis(1-(thiophen-2-yl)prop-2-yn-1-one) (5)

2,6-Diethynyl-4,8-bis((S)-3,7-dimethyloctyloxy)benzo[1,2-*b*:4,5-*b'*]dithiophene (13) (200 mg, 0.36 mmol), thiophene-2-carbonyl chloride (138 mg, 0.94 mmol), Pd(PPh₃)₄ (21 mg, 0.018 mmol) and Et₃N (15 mL) were mixed together. The resulting mixture was left under stirring for 48 h at 50 °C, then it was cooled to room temperature, hydrolyzed with saturated ammonium chloride solution (20 mL) and extracted with CH₂Cl₂ (3 × 30 mL). The combined organic phases were washed with brine (50 mL), dried over anhydrous Na₂SO₄ and the solvent was removed under vacuum. The crude product was purified by column chromatography (SiO₂, *n*-hexane/CH₂Cl₂ 1:2) to give 3,3'-(4,8-bis((S)-3,7-dimethyloctyloxy)benzo[1,2-*b*:4,5-*b'*]dithiophene-2,6-diyl)bis(1-(thiophen-2-yl)prop-2-yn-1-one) (5) (158 mg, yield 57%) as a red-orange solid. ¹H NMR (400 MHz, CDCl₃), δ (ppm): 0.90 (12H, d, *J* = 6.6 Hz), 1.03 (6H, d, *J* = 6.6 Hz), 1.16–1.45 (12H, m), 1.53–1.62 (2H, m), 1.68–1.87 (4H, m), 1.94–2.02 (2H, m), 4.33–4.42 (4H, m), 7.25 (2H, m), 7.79 (2H, d, *J* = 4.9 Hz), 7.95 (2H, s), 8.05 (2H, d, *J* = 3.7 Hz). ¹³C NMR (100 MHz, CDCl₃), δ (ppm): 19.73, 22.62, 22.71, 24.69, 27.96, 29.78, 37.30, 37.51, 39.23, 72.88, 84.79, 92.07, 120.36, 128.47, 130.45, 131.12, 132.33, 135.36, 135.69, 144.55, 144.70, 168.91. LC-MS (APCI⁺), *m/z*: 772.05 [M+H]⁺. Anal. calcd for C₄₄H₅₀O₄S₄: C, 68.53; H, 6.54; S, 16.63; found: C, 68.67; H, 6.42; S, 16.64.

2.4. Characterization

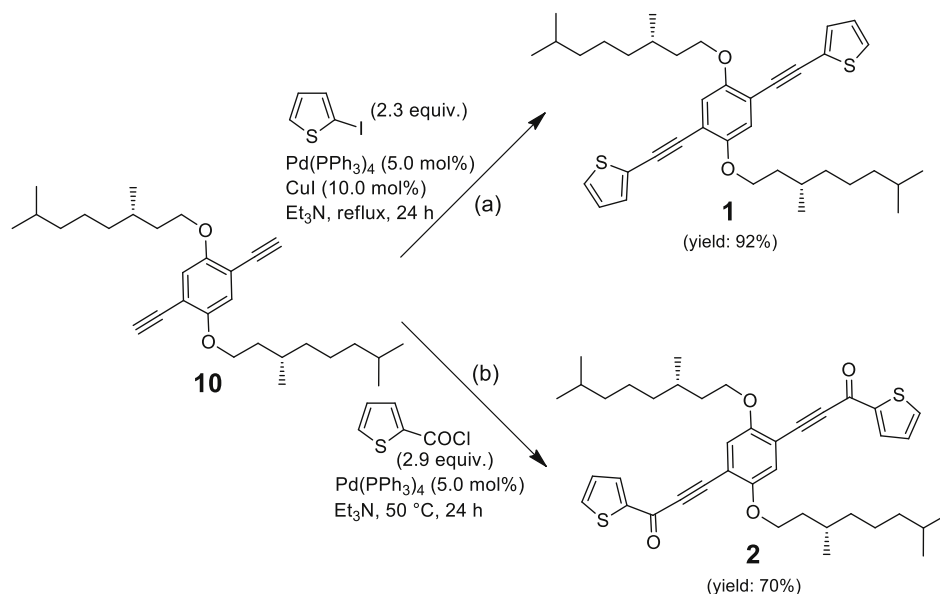
UV–Vis characterisation of the fluorophores was performed on a Shimadzu UV-2450 double beam spectrophotometer, with temperature control to within ± 0.1 °C. Fluorescence experiments were done either on a PerkinElmer LS55 spectrofluorometer or on a Horiba Jobin Yvon FluoroLog®-3 spectrofluorometer, with temperature control to within ± 0.1 °C. Stock solutions of each dye in the solvent (chloroform with 1% EtOH, toluene, acetonitrile, acetone) were typically 10^{−2} M, whereas working solutions were 10^{−4} M for absorbance and 10^{−5} M in the case of fluorescence measurements. Temperature was fixed at 23.0 °C. For all dyes, the stability of absorbance/fluorescence signal over time (several hours) was checked (not shown). Also, the absence of auto-aggregation phenomena was confirmed by the constancy of plots of the ratio between the absorbance values at two distinct wavelengths for different dye concentrations (Figs. S1–S7 in Supporting Information). Quantum yields were calculated using Quanta Horiba-Φ integrating sphere connected to a Horiba Jobin Yvon FluoroLog®-3 spectrofluorometer at $\lambda_{\text{exc}} = \lambda_{\text{max abs}}$.

PMMA thin films of dye 5 were prepared by drop-casting, i.e. pouring 1.2 mL of a CHCl₃ solution containing ~60 mg of the polymer and different contents (0.2–1.8 wt. %) of 5 on a 50 × 50 × 3 mm optically pure glass substrate (Edmund Optics Ltd BOROFLOAT window 50 × 50 TS). The glass slides were cleaned with chloroform and immersed in 6 M HCl for at least 12 h; then, they were rinsed with water, acetone and isopropanol and dried for 8 h at 120 °C. Solvent evaporation was performed on a warm hot plate (about 30 °C) and in a closed environment. The film thickness was measured by a Starrett micrometer to be 25 ± 5 μ m.

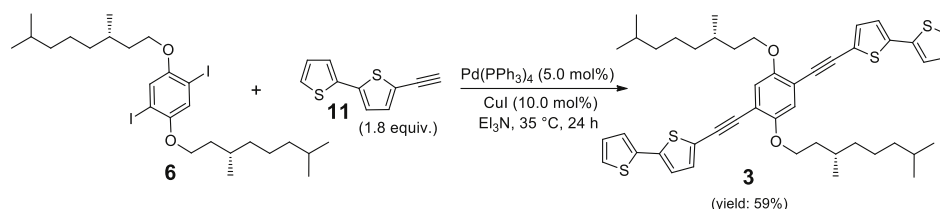
The optical efficiency of the LSC was measured by using a solar simulating lamp (ORIEL® LCS-100 solar simulator 94011A S/N: 322, AM1.5G std filter: 69 mW/cm^{−2} at 254 mm). The PV module (IXYS SLMD121H08L mono solar cell 86 × 14 mm) was connected to Keysight Technologies B2900 Series Precision Source/Measure Unit. The optical efficiency η_{opt} was evaluated from the ratio between the short circuit current measured in the case of the cell over the LSC edge (*I*_{LSC}) and short circuit current of the bare cell when perpendicular to the light source (*I*_{SC})

$$\eta_{\text{opt}} = \frac{I_{\text{LSC}}}{I_{\text{SC}} \cdot G}$$

where *G* is the geometrical factor (in our case, *G* = 16.6), which is the ratio between the area exposed to the light source and the collecting area.



Scheme 2. Synthesis of new *p*-phenylene-based fluorophores **1** and **2**.



Scheme 3. Synthesis of 1,4-bis((*S*)-3,7-dimethyloctyloxy)-2,5-bis([2,2'-bithiophen]-5-ylethynyl)benzene (**3**).

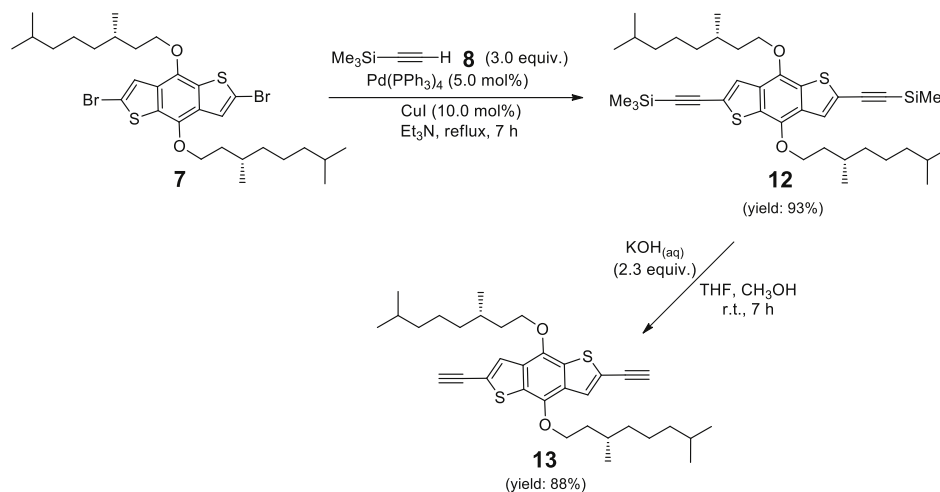
3. Results and discussion

3.1. Synthesis of new *p*-phenylene- and benzodithiophene-based fluorophores 1–5

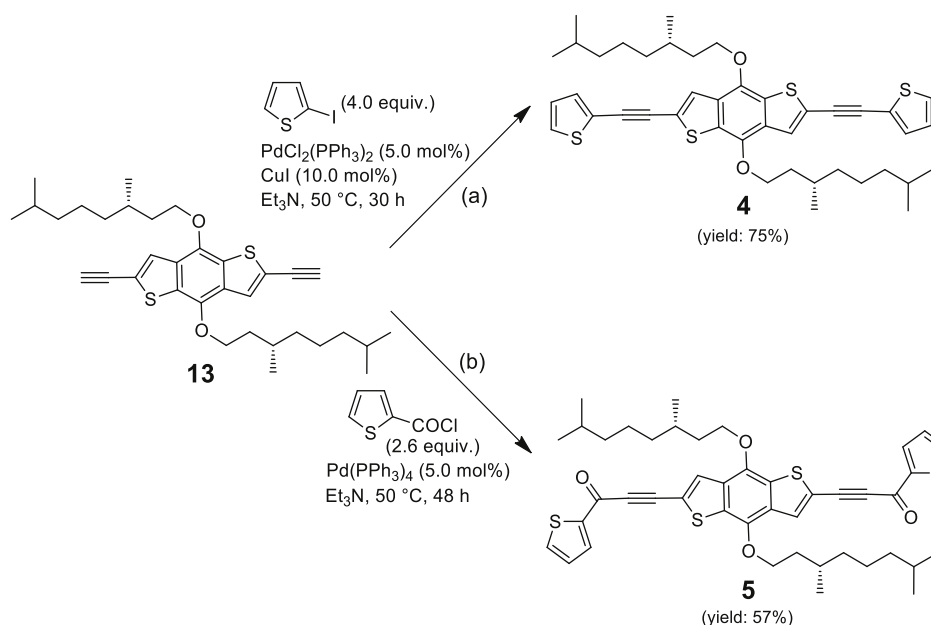
Target molecules **1–5** are new compounds and were prepared starting from, respectively, 1,4-bis(((*S*)-3,7-dimethyloctyl)oxy)-2,5-diiodobenzene (**6**) (Scheme S2 in Supporting Information) and 2,6-dibromo-4,8-bis(((*S*)-3,7-dimethyloctyl)oxy)benzo[1,2-*b*:4,5-*b'*]dithiophene (**7**) (Scheme S4 in Supporting Information). Both nuclei were characterized by a long branched chain connected to the oxygen atoms to increase the

solubility and also to reduce possible molecules aggregation in the solid state. Moreover, 3,7-dimethyloctyl moiety was easily available from citronellol after hydrogenation and subsequent bromination with *N*-bromo succinimide (Scheme S1 in Supporting Information). Initially, we treated diiodo derivative **6** with trimethylsilylacetylene (**8**) under Sonogashira reaction conditions and submitted the obtained product **9** to desilylation promoted by KOH in THF/MeOH solution to give **10** (Scheme 1).

1,4-Bis(((*S*)-3,7-dimethyloctyl)oxy)-2,5-diethynylbenzene (**10**) was then employed in the synthesis of **1** and **2** via Sonogashira reaction [36, 37] with 2-iodothiophene (Scheme 2, route a) and thiophene-2-carbonyl



Scheme 4. Synthesis of 2,6-diethynyl-4,8-bis((*S*)-3,7-dimethyloctyloxy)benzo[1,2-*b*:4,5-*b'*]dithiophene (**13**).



Scheme 5. Synthesis of new benzo[1,2-*b*:4,5-*b'*]dithiophene-based fluorophores **4** and **5**.

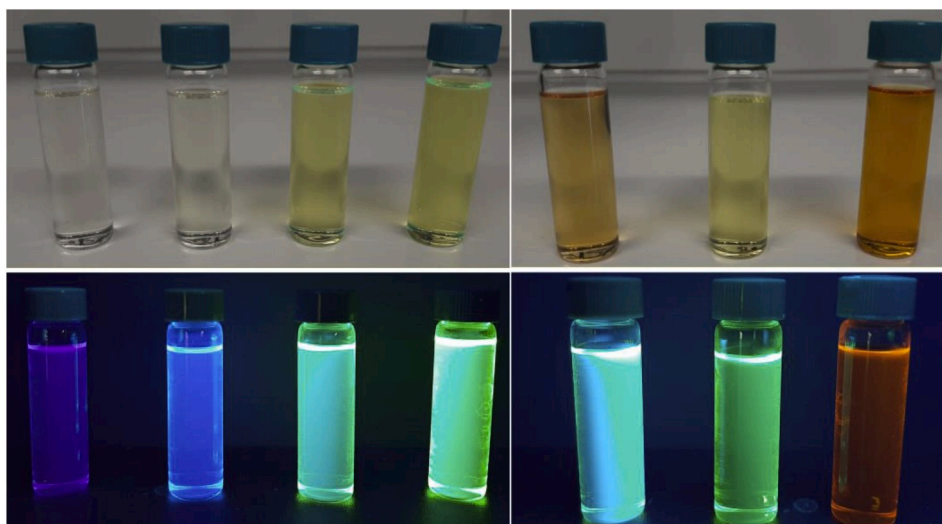


Fig. 2. Appearance of CHCl_3 solutions of our new *p*-phenylene- and benzodithiophene-based fluorophores (from left to right: **10**, **1**, **3**, **2**, **13**, **4** and **5**), illuminated with daylight (up photo) and irradiated with UV light at 365 nm (down photo).

chloride (**Scheme 2**, route b) affording the expected products in good to excellent yields.

1,4-Bis((*S*)-3,7-dimethyloctyloxy)-2,5-bis([2,2'-bithiophen]-5-ylethynyl)benzene (**3**) was generated according to a different synthetic pathway. Indeed, it was prepared by direct Sonogashira reaction of **10** with 1.8 equivalents of 5-ethynyl-2,2'-bithiophene (**11**) (**Scheme 3**). The mild experimental conditions employed during the cross-coupling reaction were due to the thermal instability of **11** which was prepared immediately before use starting from dithiophene via a three steps sequence (**Scheme S3** in Supporting Information).

Concerning the synthesis of benzo[1,2-*b*:4,5-*b'*]dithiophene (BDT) derivatives, **7** was treated with an excess of trimethylsilylacetylene (**8**), in the presence of $\text{Pd}(\text{PPh}_3)_4$ as the catalyst and Et_3N both as the base and the solvent (**Scheme 4**). After purification of the crude product, **12** was isolated in almost quantitative yield (93%). Analogously to compound **9**, removal of TMS protecting group was easily achieved by means of aqueous KOH at room temperature, which yielded diethynyl

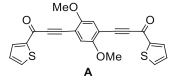
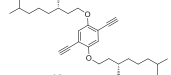
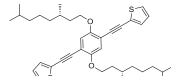
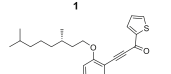
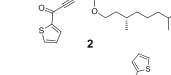
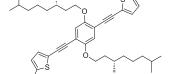
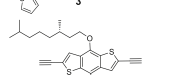
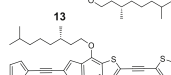
derivative **13**.

2,6-Diethynyl-4,8-bis((*S*)-3,7-dimethyloctyloxy)benzo[1,2-*b*:4,5-*b'*]dithiophene (**13**) was then employed for the synthesis of the final compounds **4** and **5**. Analogously to *p*-phenylene-based fluorophores **1**–**2**, a classic Sonogashira reaction and an acyl version of the same process were used for the formation of $\text{C}\equiv\text{C}$ -thiophene and $\text{C}\equiv\text{C}-\text{C}=\text{O}$ -thiophene bonds (**Scheme 5**).

3.2. Spectroscopic characterization in solution

We started our study with the investigation of the optical properties of fluorophores **1**–**5**, together with those of the corresponding alkynes **10** and **13**, in CHCl_3 solutions (**Fig. 2**). The main results of each compound (maximum absorbance, extinction coefficient, maximum emission, Stokes shifts and quantum yield) are collected in **Table 1**, while full absorbance and fluorescence emission spectra (**Figs. S8–S14**) and absorbance vs. concentration plots (**Figs. S15–S25**) are depicted in

Table 1Optical properties of the *p*-phenylene- and benzodithiophene-based fluorophores in CHCl₃ solution.

Compound	$\lambda_{\max \text{ abs}}$ (nm) ^[a]	$\epsilon(\lambda_{\max})$ (M ⁻¹ cm ⁻¹) ^[b]	$\lambda_{\max \text{ fl}}$ (nm) ^[c]	Stokes Shift (nm) ^[d]	Quantum yield Φ (%) ^[e]
 A	403	2.8×10^4	471	68	19.2
 10	336	0.9×10^4	377	41	17.1
 1	378	5.7×10^4	409	31	21.1
 2	334 410	4.0×10^4 2.4×10^4	472	138 62	26.0 29.7
 3	408	8.5×10^4	454	46	29.6
 13	330 395	6.4×10^4 2.1×10^4	451	121 56	44.0 44.4
 4	370 421	6.6×10^4 4.2×10^4	485	115 64	10.6 13.0
 5	386 459	5.5×10^4 2.4×10^4	581	195 122	10.5 15.3

^a Maximum of light absorbance.^b Extinction coefficient.^c Maximum of light emission; excitation wavelength is $\lambda_{\max \text{ abs}}$.^d Stokes shift is defined as $\lambda_{\max \text{ fl}} - \lambda_{\max \text{ abs}}$.^e Calculated using Quanta Horiba- Φ integrating sphere at $\lambda_{\text{exc}} = \lambda_{\max \text{ abs}}$.**Table 2**Optical properties of *p*-phenylene-based fluorophore **2** in different solvents, T = 23.0 °C.

Solvent	Polarity	$\lambda_{\max \text{ abs}}$ (nm) ^[a]	$\epsilon(\lambda_{\max})$ (M ⁻¹ cm ⁻¹) ^[b]	$\lambda_{\max \text{ fl}}$ (nm) ^[c]	Stokes Shift (nm) ^[d]	Quantum yield Φ (%) ^[e]
Toluene	2.38	331	3.8×10^4	456	125	11.8
		404	2.3×10^4		52	18.1
Chloroform	4.81	334	4.0×10^4	472	138	26.0
		410	2.4×10^4		62	29.7
Acetone	21.0	405	1.9×10^4	478	73	42.6
Acetonitrile	38.8	330	4.3×10^4	489	159	28.5
		406	2.4×10^4		83	38.9

^a Maximum of light absorbance.^b Extinction coefficient.^c Maximum of light emission; excitation wavelength is $\lambda_{\max \text{ abs}}$.^d Stokes shift is defined as $\lambda_{\max \text{ fl}} - \lambda_{\max \text{ abs}}$.^e Calculated using Quanta Horiba- Φ integrating sphere at $\lambda_{\text{exc}} = \lambda_{\max \text{ abs}}$.**Supporting Information.**

In general, we observed that the extension of conjugation produced significant bathochromic and auxochromic effects (the latter in the case of **1–3**). As for the species containing the hydroquinone nucleus, by comparing the data on **10** and **1** (see also Figs. S8–S9), we found that the insertion of thiophenes on the acetylenic positions produced an increase in both absorption and emission properties with a quantum yield (Φ) rising to 20%, even in the presence of a lower Stokes shift. This feature can be possibly addressed to the increase in molecular rigidity provided by the enhanced molecular conjugation that, in turn, reduced the probability of de-excitation processes via non-radiative pathways [38].

Di-thiophene units further increased Φ up to 30% and enhanced the bathochromic effect (Fig. S11). Carbonyl groups slightly increased Φ being supported by the larger red-shift of the emission compared to that of the absorption, so that the superimposition between absorbance spectrum and emission one was diminished (Fig. S10); interestingly, the presence in **2** of long aliphatic chains favoured solubilisation and produced a quantum yield increase with respect to the methoxy species **A** previously described [35]. These features let fluorophore **2** be a better candidate for application as LSC.

The dependence of the optical features of **2** on the solvent was then tested (Table 2 and Fig. 3). The performances increased by increasing

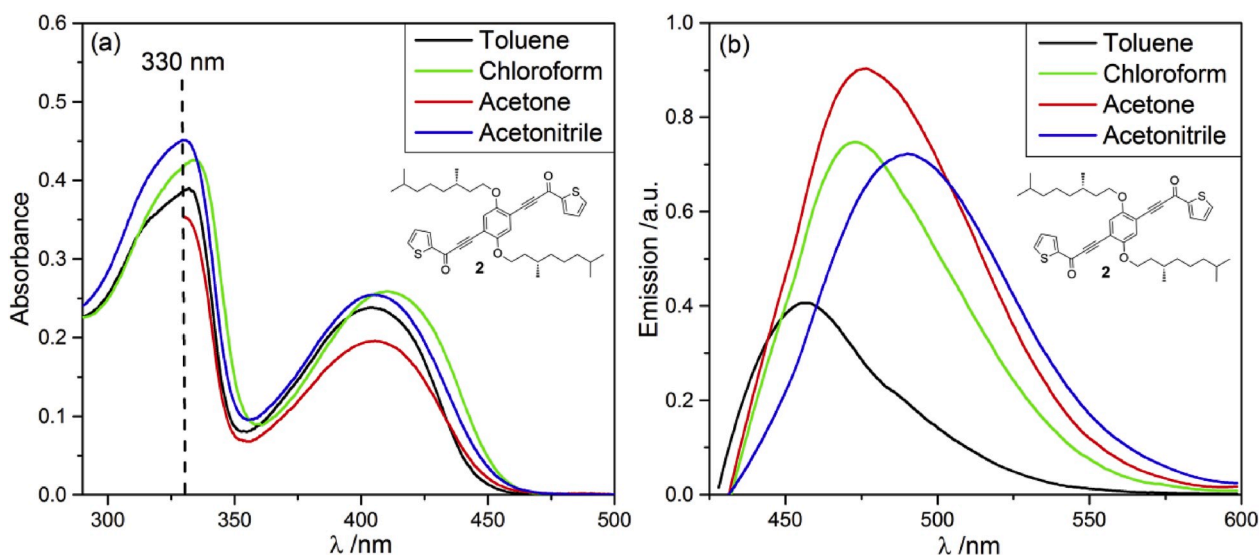


Fig. 3. a) Absorbance spectra of **2** in different solvents; concentration = 1.0×10^{-5} M. b) Emission spectra of **2** in different solvents; concentration = 6.5×10^{-8} M. For acetone cut-off at 330 nm.

Table 3

Optical properties of benzodithiophene-based fluorophore **5** in different solvents, T = 23.0 °C.

Solvent	Polarity	$\lambda_{\text{max abs}}$ (nm) ^[a]	$\epsilon(\lambda_{\text{max}})$ (M ⁻¹ cm ⁻¹) ^[b]	$\lambda_{\text{max fl}}$ (nm) ^[c]	Stokes Shift (nm) ^[d]	Quantum yield Φ (%) ^[e]
Toluene	2.38	381	5.1×10^4	552	171	60.9
		459	2.1×10^4		93	87.0
Chloroform	4.81	386	5.5×10^4	581	195	10.5
		459	2.4×10^4		122	15.3
Acetone	21.0	379	5.6×10^4	574	195	2.7
		450	2.2×10^4		124	4.7
Acetonitrile	38.8	379	4.3×10^4	/	/	/
		445	2.4×10^4			

^a Maximum of light absorbance.

^b Extinction coefficient.

^c Maximum of light emission; excitation wavelength is $\lambda_{\text{max abs}}$.

^d Stokes shift is defined as $\lambda_{\text{max fl}} - \lambda_{\text{max abs}}$.

^e Calculated using Quanta Horiba- Φ integrating sphere at $\lambda_{\text{exc}} = \lambda_{\text{max abs}}$.

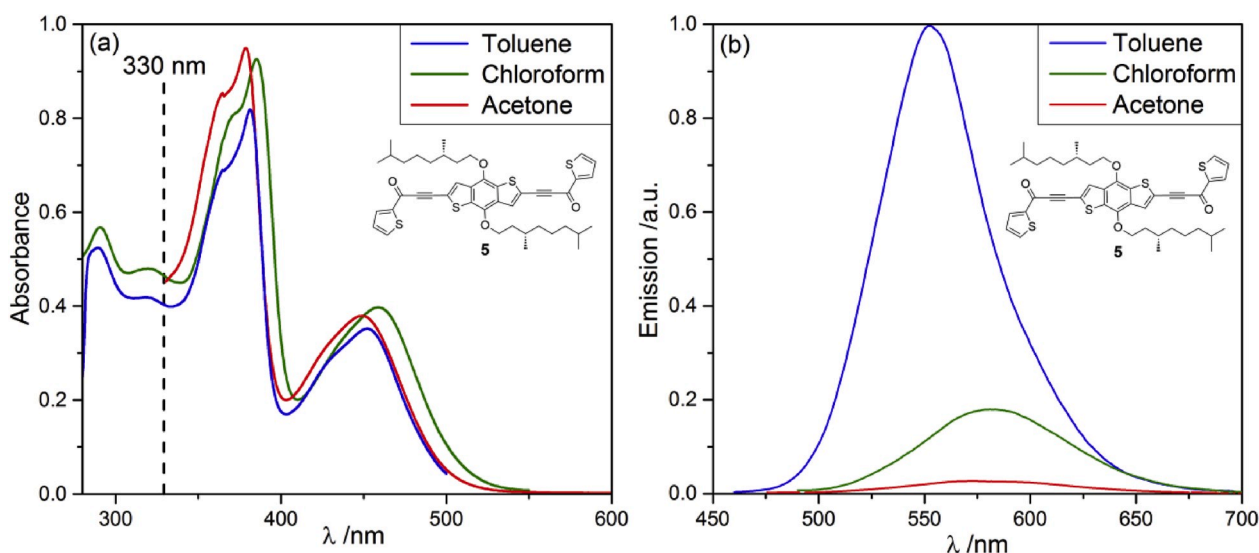


Fig. 4. a) Absorbance spectra of **5** in different solvents; concentration = 1.6×10^{-5} M. b) Emission spectra of **5** in different solvents; concentration = 1.2×10^{-6} M. For acetone cut-off at 330 nm.

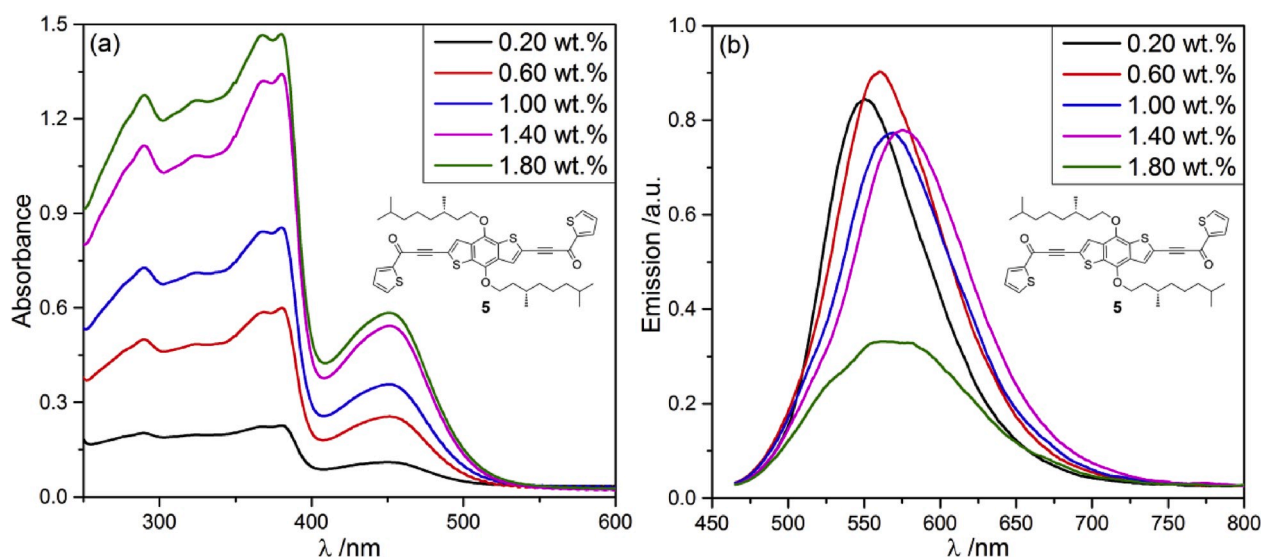


Fig. 5. Absorbance (a) and emission (b) spectra of **5** as thin films in PMMA (thickness $25 \pm 5 \mu\text{m}$) at different dye concentrations (0.2–1.8 wt. %). For emission spectra, excitation wavelength is $\lambda_{\text{max abs}}$.

the solvent polarity. In particular, absorption data did not change much while $\lambda_{\text{max fl}}$ and Φ increased. Fig. S26 in Supporting Information showed the appearance of solutions of **2** in the different solvents, together with a Lippert-Mataga plot [39] to enlighten its solvatochromism.

Concerning the species with benzodithiophene core (Table 1 and Figs. S12–S14), the increase of π -conjugation from **13** to **4** and **5** did not reflect in a quantum yield increase which, instead, is significantly decreased. This is likely to be ascribed to the rotation around the alkyne-thiophene bond. The molar extinction coefficient remained almost unchanged, but Stokes shift increased and reached 122 nm for compound **5**. Therefore, despite a low quantum yield, the very low superimposition of absorption and emission profiles let **5** be the best candidate for application in LSCs. Also, light emission of **5** is red-shifted until the region of maximum traditional silica cells efficiency ($\lambda > 500 \text{ nm}$). Therefore, similarly to **2**, fluorophore **5** was selected for further characterisation in different solvents (Table 3 and Fig. 4).

The obtained results (see also Fig. S27 for the appearance of solutions of **5** and Lippert-Mataga plot) showed that a polarity increase produced a marked decrease in fluorophore efficiency. In particular, fluorescence emission is lost in acetonitrile, and the same sharp drop is observed for Φ values. On the whole, compound **5** seems a good candidate for LSCs applications due to light emission in the red, good quantum yield in toluene (which is close to the PMMA matrix as for polarity), possibly high dye/matrix compatibility grace to long and branched alkyl chains that endow high solubility into organic solvents.

3.3. Spectroscopic characterization of benzodithiophene-based fluorophore **5** in PMMA films

Therefore, dye **5** was selected for additional tests as thin films into the polymeric PMMA matrix, prepared by casting on a $50 \times 50 \times 3 \text{ mm}$ glass substrate 1.2 mL of a chloroform solution containing 60 mg of PMMA and different contents (0.2–1.8 wt. %) of **5**. The absorption features of **5**/PMMA films (thickness $25 \pm 5 \mu\text{m}$) are displayed in Fig. 5a. Compound **5** in PMMA showed absorption maxima at about 380 and 450 nm, appearing mostly similar to that recorded in toluene solution (i. e., 381 and 459 nm, respectively) and with absorbance intensities that increased regularly with fluorophore content. Notably, no evident absorption bands attributed to the formation of **5** aggregates can be noticed, most probably thanks to the compatibilizing effect provided by the alkyl chains linked to the benzodithiophene core.

Table 4

Optical properties of **5**/PMMA thin films at different dye concentrations (0.2–1.8 wt. %), $T = 23.0^\circ\text{C}$.

Concentration (wt. %)	$\lambda_{\text{max abs}}$ (nm) ^[a]	$\lambda_{\text{max fl}}$ (nm) ^[b]	Stokes Shift (nm) ^[c]	Quantum yield Φ (%) ^[d]
0.20	450	550	100	53.3
0.60	450	560	110	33.8
1.00	450	568	118	27.2
1.40	450	575	125	20.1
1.80	450	567	117	16.4

^a Maximum of light absorbance.

^b Maximum of light emission; excitation wavelength is $\lambda_{\text{max abs}}$.

^c Stokes shift is defined as $\lambda_{\text{max fl}} - \lambda_{\text{max abs}}$.

^d Calculated using Quanta Horiba- Φ integrating sphere at $\lambda_{\text{exc}} = \lambda_{\text{max abs}}$.

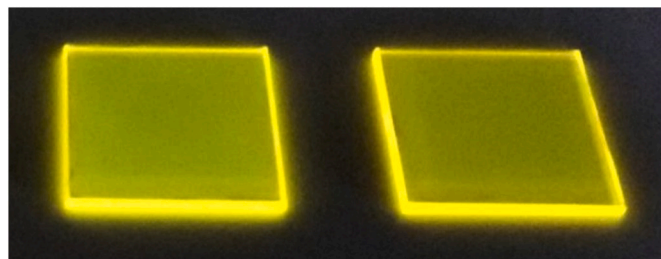


Fig. 6. Optical micrographs of **5**/PMMA thin films with 1.0 wt. % (left) and 1.4 wt. % (right) dye content, under excitation at 366 nm. Film size = $5 \times 5 \text{ mm}^2$.

On the contrary, **5**/PMMA films displayed emission features adversely affected by the fluorophore concentration (Fig. 5b). When dispersed in PMMA at a concentration of 0.2 wt. %, **5** displayed a bright fluorescence emission peaked at 550 nm with a Stokes shift of 100 nm and $\Phi = 53.3\%$ (Table 4), again in agreement with results collected in toluene solutions.

Above this content, the fluorescence band did not display any evident quenching albeit a significant decrease of Φ up to 20% was detected at 1.4 wt. % concentration and flanked by a red-shift of its maximum of 15 nm, which is possibly addressed to auto-absorption phenomena [40–42]. Actually, the enhanced absorption of light by the increased amount of fluorophores added in the polymer matrix progressively contributed in the absorption of part of the emission placed at

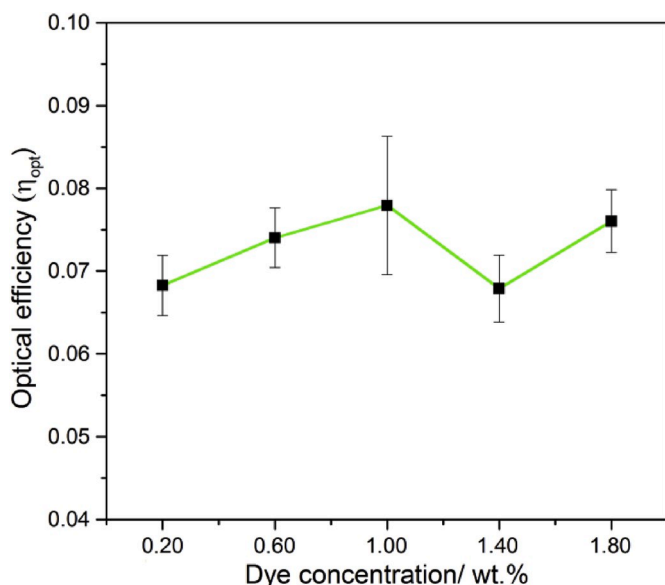


Fig. 7. Optical efficiencies (η_{opt}) of 5/PMMA thin films as a function of fluorophore concentration.

high energy (inner-filter effect), *i.e.* close to the tail of the absorption spectrum. This phenomenon eventually caused a substantial red-shift of the emission due to the decreased contribution of the high-energy portion of the fluorescence band. Nevertheless, the emission of 5 in PMMA thin films persisted at the highest content (1.8 wt. %), *i.e.* showing a broad fluorescence peaked at 567 nm and with a Φ of 16.4%. Inspections of optical micrographs of 5/PMMA samples taken under the excitation of a long-range UV lamp at 366 nm (Fig. 6) revealed the absence of any macroscopic phase segregation of 5 within the polymer matrix also at high fluorophore content, that is possibly addressed to the compatibilizing characteristics of the alkyl chains linked to the chromophoric core. Fluorescence quenching of 5 within PMMA can be therefore addressed to auto-absorption phenomena (*i.e.*, inner-filter effects), that is possibly neglecting the influence of the aggregation-caused quenching phenomenon.

3.4. Optical efficiency of benzodithiophene-based fluorophore 5 in PMMA films

The optical performances of the 5/PMMA thin films as luminescent solar concentrator (LSC) were determined by covering an optically pure $50 \times 50 \times 3$ mm glass with the luminescent film and using a Si-based PV cell attached to one edge of the solar collector.

The data acquired (Fig. 7) showed that the optical efficiency (η_{opt}) increased with 5 content and leveled off for concentration higher than 1 wt. %, possibly due to adverse dissipative issues such as auto-absorption phenomena that were particularly effective for the sample containing 1.4 wt. % of the fluorophore. At this content, the contribution of fluorescence quenching to η_{opt} resulted particularly stronger than the beneficial effect of solar harvesting provided by the amount of 5 dispersed into the film. Nevertheless, the maximum optical efficiency of about 8% was obtained and resulted comparable with those of PMMA thin films containing Lumogen Red in the same range of concentration and determined with the same laboratory setup [43].

4. Conclusion

In summary, an easy sequence for the preparation of new fluorophores containing *p*-phenylene or benzodithiophene nucleus based on Sonogashira cross-coupling reactions has been developed. All compounds were generated in good to high yields and resulted soluble in the

investigated organic solvents thanks to the alkyl chains linked to the chromophoric units. Spectroscopic investigations in solution evidenced that the fluorophore based on the benzodithiophene core bearing the carbonyl-thiophene residues appeared as the most promising for LSCs applications thanks to the good quantum yield ($> 60\%$ in toluene), large Stokes shift (> 90 nm) and emission peaked at 550 nm. PMMA thin films containing 1 wt. % of the selected fluorophore showed the highest optical efficiency of 8% that is equivalent to that recorded for films containing the red-emitting Lumogen Red and therefore promising for solar collectors applications.

Declaration of competing interest

The authors declare that they have no known competing financial interests or personal relationships that could have appeared to influence the work reported in this paper.

CRediT authorship contribution statement

Gianluigi Albano: Data curation. **Tony Colli:** Data curation. **Tarita Biver:** Supervision. **Laura Antonella Aronica:** Supervision. **Andrea Pucci:** Supervision.

Acknowledgements

Funding from University of Pisa – PRA_2017_28 is gratefully acknowledged.

Appendix A. Supplementary data

Supplementary data to this article can be found online at <https://doi.org/10.1016/j.dyepig.2020.108368>.

References

- [1] Markvart T, Castañer L. Principles of solar cell operation. In: Kalogirou SA, editor. McEvoy's handbook of photovoltaics: fundamentals and applications. Academic Press; 2017. p. 3–28.
- [2] Khamooshi M, Salati H, Egelioglu F, Hooshyar Faghiri A, Tarabishi J, Babadi S. A review of solar photovoltaic concentrators. *Int J Photoenergy* 2014;2014: 958521.
- [3] Shanks K, Senthilarasu S, Mallick TK. Optics for concentrating photovoltaics: trends, limits and opportunities for materials and design. *Renew Sustain Energy Rev* 2016;60:394–407.
- [4] Katz EA, Visoly-Fisher I, Feuermann D, Tenne R, Gordon JM. Concentrated sunlight for materials synthesis and diagnostics. *Adv Mater* 2018;30(41):1800444.
- [5] Sala G, Antón I. Photovoltaic concentrators. In: Luque A, Hegedus S, editors. *Handbook of photovoltaic science and engineering*. second ed. John Wiley & Sons, Ltd; 2011. p. 402–51.
- [6] Siecker J, Kusaka K, Numbi BP. A review of solar photovoltaic systems cooling technologies. *Renew Sustain Energy Rev* 2017;79:192–203.
- [7] van Sark WGHM, Barnham KWJ, Slooff LH, Chatten AJ, Büchtemann A, Meyer A, et al. Luminescent Solar Concentrators - a review of recent results. *Optic Express* 2008;16(26):21773–92.
- [8] Rowan BC, Wilson LR, Richards BS. Advanced material concepts for luminescent solar concentrators. *IEEE J Sel Top Quant Electron* 2008;14(5):1312–22.
- [9] Debije MG, Verbunt PPC. Thirty years of luminescent solar concentrator research: solar energy for the built environment. *Adv Energy Mater* 2012;2(1):12–35.
- [10] Tonezzer M, Gutierrez D, Vincenzi D. Luminescent solar concentrators – state of the art and future perspectives. In: Tiwari A, Boukherroub R, Sharon M, editors. *Solar cell nanotechnology*. Scrivener Publishing LLC; 2014. p. 293–315.
- [11] Reissfeld R. Luminescent solar concentrators and the ways to increase their efficiencies. In: Levy D, Zayat M, editors. *The sol-gel handbook*. Wiley-VCH Verlag GmbH & Co.; 2015. p. 1281–308.
- [12] Moraitis P, Schropp REI, van Sark WGHM. Nanoparticles for luminescent solar concentrators - a review. *Opt Mater* 2018;84:636–45.
- [13] Rafiee M, Chandra S, Ahmed H, McCormack SJ. An overview of various configurations of Luminescent Solar Concentrators for photovoltaic applications. *Opt Mater* 2019;91:212–27.
- [14] Li Y, Zhang X, Zhang Y, Dong R, Luscombe CK. Review on the role of polymers in luminescent solar concentrators. *J Polym Sci, Part A: Polym Chem* 2019;57(3): 201–15.
- [15] Zhou Y, Zhao H, Ma D, Rosei F. Harnessing the properties of colloidal quantum dots in luminescent solar concentrators. *Chem Soc Rev* 2018;47(15):5866–90.

- [16] Sutherland BR. Cost competitive luminescent solar concentrators. *Joule* 2018;2(2): 203–4.
- [17] Ma Y, Zhang Y, Yu WW. Near infrared emitting quantum dots: synthesis, luminescence properties and applications. *J Mater Chem C* 2019;7(44):13662–79.
- [18] You Y, Tong X, Wang W, Sun J, Yu P, Ji H, et al. Eco-friendly colloidal quantum dot-based luminescent solar concentrators. *Adv Sci* 2019;6(9):1801967.
- [19] Correia SFH, de Zea Bermudez V, Ribeiro SJL, André PS, Ferreira RAS, Carlos LD. Luminescent solar concentrators: challenges for lanthanide-based organic–inorganic hybrid materials. *J Mater Chem* 2014;2(16):5580–96.
- [20] Long J, Guari Y, Ferreira RAS, Carlos LD, Larionova J. Recent advances in luminescent lanthanide based Single-Molecule magnets. *Coord Chem Rev* 2018; 363:57–70.
- [21] Salem AI, Mansour AF, El-Sayed NM, Bassyouni AH. Outdoor testing and solar simulation for oxazine 750 laser dye luminescent solar concentrator. *Renew Energy* 2000;20(1):95–107.
- [22] Chen Y, Wan X, Long G. High performance photovoltaic applications using solution-processed small molecules. *Acc Chem Res* 2013;46(11):2645–55.
- [23] Green AP, Butler KT, Buckley AR. Tuning of the emission energy of fluorophores using solid state solvation for efficient luminescent solar concentrators. *Appl Phys Lett* 2013;102(13):133501.
- [24] Zhou W, Wang M-C, Zhao X. Poly(methyl methacrylate) (PMMA) doped with DCJTb for luminescent solar concentrator applications. *Sol Energy* 2015;115: 569–76.
- [25] Liu C, Li B. Multiple dyes containing luminescent solar concentrators with enhanced absorption and efficiency. *J Optic* 2015;17(2). 025901.
- [26] Lucarelli J, Lessi M, Manzini C, Minei P, Bellina F, Pucci A. N-alkyl diketopyrrolopyrrole-based fluorophores for luminescent solar concentrators: effect of the alkyl chain on dye efficiency. *Dyes Pigments* 2016;135:154–62.
- [27] Bellina F, Manzini C, Marianetti G, Pezzetta C, Fanizza E, Lessi M, et al. Colourless p-phenylene-spaced bis-azoles for luminescent concentrators. *Dyes Pigments* 2016; 134:118–28.
- [28] Marianetti G, Lessi M, Barone V, Bellina F, Pucci A, Minei P. Solar collectors based on luminescent 2,5-diarylimidazoles. *Dyes Pigments* 2018;157:334–41.
- [29] Papucci C, Geervliet TA, Franchi D, Bettucci O, Mordini A, Reginato G, et al. Green/yellow-emitting conjugated heterocyclic fluorophores for luminescent solar concentrators. *Eur J Org Chem* 2018;2018(20–21):2657–66.
- [30] Albano G, Aronica LA, Biver T, Detti R, Pucci A. Tris-Ethynylphenyl-amine fluorophores: synthesis, characterisation and test of performances in luminescent solar concentrators. *ChemistrySelect* 2018;3(6):1749–54.
- [31] Achelle S, Rodríguez-López J, Guen FR-I. Photoluminescence properties of aryl-, arylvinyl-, and arylethynylpyrimidine derivatives. *ChemistrySelect* 2018;3(6): 1852–86.
- [32] Albano G, Lissia M, Pescitelli G, Aronica LA, Di Bari L. Chiroptical response inversion upon sample flipping in thin films of a chiral benzo[1,2-b:4,5-b'] dithiophene-based oligothiophene. *Mater Chem Front* 2017;1(10):2047–56.
- [33] Albano G, Salerno F, Portus L, Porzio W, Aronica LA, DiBari L. Outstanding chiroptical features of thin films of chiral oligothiophenes. *ChemNanoMat* 2018;4 (10):1059–70.
- [34] Albano G, Górecki M, Pescitelli G, Di Bari L, Jávorfí T, Hussain R, et al. Electronic circular dichroism imaging (CDi) maps local aggregation modes in thin films of chiral oligothiophenes. *New J Chem* 2019;43(36):14584–93.
- [35] Albano G, Colli T, Nucci L, Charaf R, Biver T, Pucci A, et al. Synthesis of new bis[1-(thiophenyl)propynones] as potential organic dyes for colorless luminescent solar concentrators (LSCs). *Dyes Pigments* 2020;174:108100.
- [36] Chinchilla R, Nájera C. Recent advances in Sonogashira reactions. *Chem Soc Rev* 2011;40(10):5084–121.
- [37] Albano G, Aronica LA. Acyl Sonogashira cross-coupling: state of the art and application to the synthesis of heterocyclic compounds. *Catalysts* 2020;10(1):25.
- [38] Hamilton G, Sanabria H. Chapter 6 - multiparameter fluorescence spectroscopy of single molecules. In: Johnson CK, editor. *Spectroscopy and dynamics of single molecules*. Elsevier; 2019. p. 269–333.
- [39] Lippert E. Spektroskopische Bestimmung des Dipolmomentes aromatischer Verbindungen im ersten angeregten singulettzustand. *Z Elektrochem* 1957;61(8): 962–75.
- [40] De Nisi F, Francischello R, Battisti A, Panniello A, Fanizza E, Striccoli M, et al. Red-emitting AIEgen for luminescent solar concentrators. *Mater Chem Front* 2017;1(7): 1406–12.
- [41] Gianfaldoni F, De Nisi F, Iasilli G, Panniello A, Fanizza E, Striccoli M, et al. A push–pull silafluorene fluorophore for highly efficient luminescent solar concentrators. *RSC Adv* 2017;7(59):37302–9.
- [42] Mori R, Iasilli G, Lessi M, Muñoz-García AB, Pavone M, Bellina F, et al. Luminescent solar concentrators based on PMMA films obtained from a red-emitting ATRP initiator. *Polym Chem* 2018;9(10):1168–77.
- [43] Geervliet TA, Gavrila I, Iasilli G, Picchioni F, Pucci A. Luminescent solar concentrators based on renewable polyester matrices. *Chem Asian J* 2019;14(6): 877–83.